Korean J. Chem. Eng., 36(10), 1626-1636 (2019)
DOI: 10.1007/s11814-019-0363-2

pISSN: 0256-1115
eISSN: 1975-7220

Dissolution of lignocellulosic biomass in ionic liquid-water media: Interpretation from solubility parameter concept

Gayatri Gogoi*, and Swapnali Hazarika*,**,†**

*Chemical Engineering Group, Engineering Science and Technology Division (ESTD), CSIR North East Institute of Science & Technology, Jorhat-785006, Assam, India
**Academy of Scientific and Industrial Research, CSIR NEIST Campus
(*Received 3 May 2019 • accepted 15 August 2019*)

Abstract−Lignocellulosic biomass, Water hyacinth (*Eichornia crassipes*) was pretreated with ionic-liquid (IL)-water mixture using ILs, 1-butyl-3-methylimidazolium acetate [BMIM]OAc, 1-butyl-3-methylimidazolium chloride [BMIM]Cl, 1-butyl-3-methylimidazolium bromide [BMIM]Br and 1-butyl-3-methylimidazolium tetrafluoroborate [BMIM]TFB. Effects of IL anions, IL content, temperature, time and particle size of biomass on dissolution and recovery of lignin were examined and the conditions were optimized. Biomass dissolution and yield of lignin recovery in IL-water mixtures with different anions of 1-butyl-3-methyl imidazolium based ILs follows the order, [BMIM]OAc>[BMIM]Cl>[BMIM]Br>[BMIM]TFB. The role of IL-water mixture for dissolution and recovery of lignin was investigated by characterizations using XRD, SEM, FTIR, TGA and XRF spectroscopy. The Hildebrand solubility parameters of biomass component (lignin) and IL-water mixtures were examined using intrinsic viscosity method. On applying the concept of Hildebrand solubility parameter for dissolution of the biomass in all the IL-water mixtures the results were consistent with the experimental results, which suggests that Hildebrand solubility parameter concept can be applied as primary information in choosing the appropriate solvent for biomass dissolution.

Keywords: Lignocellulosic Biomass, Ionic Liquid, Dissolution, Lignin, Hildebrand Solubility Parameter

INTRODUCTION

The excessive use of non-renewable energy resources accelerates global problems such as deterioration of the environment and human health problems. Therefore utilization of renewable energy resources has become a major concern for sustainable development and environmental protection [1,2]. In this context lignocellulosic biomass, which is composed of mainly cellulose, hemicelluloses and lignin is considered as attractive renewable energy resource owing to its abundance and relatively low cost. Water hyacinth (*Eichornia crassipes*), originating from the Amazon basin, a widespread aquatic weed that affects the water bodies, has a great potential as renewable raw material or feedstock for bioethanol production and for other applications. Pretreatment of the water hyacinth is necessary to improve the accessibility of the cellulose for hydrolytic enzymes. Water hyacinth is comprised mainly of high amount of cellulose (18-31%), hemicelluloses (18-43%) and lignin (7-26%) [3]. Further chemical and biotechnological conversion of cellulose and hemicelluloses derived from water hyacinth into value added products is also possible [4-6]. Along with this a number of relevant studies have also been reported for chemical and biotechnological conversion of cellulosic materials through in situ esterification of microalgae [7-9]. While lignin, a complex polymer consisting of phenyl propanoid units comprised mainly of coniferyl, sinapyl and p-coumaryl alcohols is an aromatic biopolymer that can be used as the feedstock for renewable fuel and chemicals [10,11]. Lignin along with cellulose and hemicellulose forms an extensive three-dimensional network that resists further chemical and enzymatic degradation. Inhibitory effect of lignin also occurs due to the adsorption of enzyme on lignin [12]. Therefore, removal of lignin is very necessary during pretreatment of biomass so as to increase the enzymatic hydrolysis of lignocellulosic biomass and further utilization. Lignin extracted from biomass can be predominantly utilized as secondary fuel, binder, dispersant, emulsifier and sequestrant and also has a great potential for its conversion into value added products like mixed alcohols, aromatic chemicals or high octane fuel and carbon fibers. Thus lignin can serve as a renewable and sustainable material that can significantly improve the economics of a biorefinery [13,14].

Many researchers have explored the potential of various ILs as pretreatment solvent for lignocellulosic biomass due to the unique features of ILs such as low volatility, low flammability, good thermal stability, tunable viscosity and other properties like hydrophobicity, polarity and solvent power [15-19]. However, several drawbacks are associated with the utilization of ILs that are needed to be resolved such as slow dissolution rate, high costs of ILs and greater viscosity of ILs. Therefore, utilization of IL-water mixture as a pretreatment solvent for the lignocellulosic biomass can be considered as an advanced step towards improved process of dissolving lignocellulosic biomass. The addition of water to the IL lowers the viscosity and thus lowers processing cost as well as enhances the ease of recyclability of the IL, which makes it a promising technol-

†To whom correspondence should be addressed.
E-mail: shrrljt@yahoo.com

ogy for pretreatment of lignocellulosic biomass [20-22]. A number of studies have been reported on dissolution of lignocelluloses using IL-water mixtures [20-24]. Viscosity of IL plays an important role in the dissolution speed and addition of water decreases the viscosity of IL. But it is reported that decrease in viscosity of IL significantly reduces the cellulose solubility in it [25,26]. Interestingly, there is a significance increase in the solubility of lignin on decreasing the viscosity of IL [20,27]. Brandt et al. [21] studied the effect of nature of anion of ILs on treating the lignocellulosic biomass with butyl methyl imidazolium based IL-water mixtures having different anions. For a solvent mixture having IL content of 80 wt%, the delignification was found to be highest for IL having anion hydrogen sulfate followed by methanesulfonate, acetate and chloride. A different study also found a strong correlation between delignification and IL content during the pretreatment of legume straw using an IL-water mixture [22].

The objective of this work is to verify the feasibility of dissolution of lignocellulosic components, mainly lignin, of water hyacinth in IL-water mixtures. Thus this work provides an efficient and optimized process of lignin dissolution in IL-water mixture and also correlates the experimental observations with the theoretical interpretations obtained from Hildebrand solubility parameter concept, which has not yet been reported, to the best of our knowledge. Hildebrand solubility parameter has been used as an important factor in choosing a proper solvent for the dissolution process, which is a mathematical value that denotes the strength of the interactions between solvent molecules. However, there is similar kind of study investigating the dissolution behavior of biomass in IL-water mixtures using Hansen solubility parameters [28]. But that study concluded that Hansen solubility parameter theory aids in searching an appropriate range of ionic liquid content for the IL-water mixtures, while the theory is inappropriate for evaluating the effects of the IL type on lignin solubility as evaluated from the inconsistency of the experimental results with the theoretical results. A much better explanation for using Hildebrand solubility parameter theory is obtained from further studies of Hansen solubility parameters [29] in which it was found that the radius of interaction calculated from Hansen solubility parameters, representing a distance between two sets of parameters of solute and solvent, provides significant information and agrees well with the results from the Hildebrand solubility parameter. Thus, it may be concluded that the Hildebrand solubility parameter is useful for solvent selection and for explanation of dissolution behavior. The Hildebrand can be defined as the square root of the cohesive energy density (CED), the amount of energy necessary to disrupt the interactions among molecules (ΔU) per molar volume (V), which is equal to the square root of the difference of dissolution enthalpy (ΔH) and ideal gas constant (R) timing with temperature (T) per molar volume (V) [30].

$$\delta_H = \mathrm{CED}^{\frac{1}{2}} = \left(\frac{\Delta U}{V}\right)^{\frac{1}{2}} = \left(\frac{\Delta H - RT}{V}\right)^{\frac{1}{2}} \quad (1)$$

The Hildebrand solubility parameter (δ_H) can be evaluated using several methods: heat vaporization (ΔH_v)-temperature data, solubility measurement, osmotic pressure, turbidimetric titration, swelling, inverse gas chromatography, and intrinsic viscosity [31,32]. Among these, intrinsic viscosity is found to be most effective for measuring the solubility parameters of components with low or no volatility such as polymers, and ionic liquids [33]. The Hildebrand solubility parameter of the solvent that gives the highest intrinsic viscosity value of the solute is the Hildebrand solubility parameter of the solute. Thus, the highest intrinsic viscosity value shows the highest mutual compatibility among solute and solvent [30,33]. We investigated the Hildebrand solubility parameters of different IL-water mixtures so as to choose the favorable solvent for dissolution. According to Hildebrand solubility parameter concept, a solvent having similar solubility parameter with that of the solute provides better dissolution, so it is essential to determine the Hildebrand solubility parameters of solvent mixtures and biomass component to ensure the selection of a suitable solvent.

EXPERIMENTAL

1. Materials

Fresh water hyacinth (*Eichhronia crassipes*) samples collected from Jorhat district, Assam, India were washed with water to remove extraneous materials. The leaves and stalks were dried in sunlight and then smashed by grinder to attain a particle size in the range of 150-500 micron. All the four ILs, 1-butyl-3-methyl imidazolium acetate [BMIM]OAc, 1-butyl-3-methyl imidazolium chloride [BMIM]Cl, 1-butyl-3-methyl imidazolium bromide [BMIM]Br and 1-butyl-3-methyl imidazolium tetrafluoroborate [BMIM]TFB were procured from Sigma Aldrich, USA. Standard lignin (alkaline, >99 wt%) was supplied from TCI, Japan. Analytical grade solvents having differ-

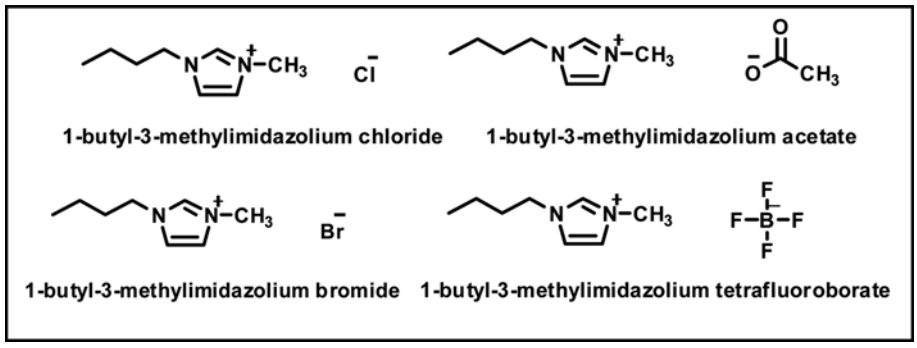

Fig. 1. Chemical structures of the ILs.

ent Hildebrand solubility parameters, i.e., 2-butanol (22.2 $MPa^{1/2}$), 2-propanol (23.5 $MPa^{1/2}$), 1-propanol (24.5 $MPa^{1/2}$), dimethyl formamide (24.8 $MPa^{1/2}$), nitromethane (25.1 $MPa^{1/2}$), allyl alcohol (25.7 $MPa^{1/2}$), ethanol (26.5 $MPa^{1/2}$), dimethyl sulfoxide (26.7 $MPa^{1/2}$), propylene carbonate (27.3 $MPa^{1/2}$), 2-pyrrolidone (28.4 $MPa^{1/2}$), methanol (29.6 $MPa^{1/2}$), diethylene glycol (29.9 $MPa^{1/2}$), ethanolamine (31.3 $MPa^{1/2}$), and water (47.9 $MPa^{1/2}$) were procured from Sigma-Aldrich. The chemical structures of the ILs used are depicted in Fig. 1.

2. Treating Water Hyacinth Samples Using IL-water Mixture

All the four ionic liquids, [BMIM]OAc, [BMIM]Cl, [BMIM]Br and [BMIM]TFB and deionized water, were mixed to form solvents according to the experimental requirements (i.e., 20-100 wt% of IL). In a round bottom flask 1 g biomass sample was mixed with 20 g of IL-water mixtures. The flask was heated and the mixture was allowed to stir with the help of a magnetic stirrer for different combinations of time and temperature ranging from 303-393 K for 1-4 h to dissolve the sample in the mixture of solvent. After stirring under heat for desired time and temperature, the mixture was allowed to cool to room temperature. Then the biomass mixture was filtered followed by separation into insoluble residue and filtrate. Vacuum filtration of the insoluble residue was done to wash it using deionized water and the residue was dried and weighed. The weight loss of the water hyacinth in the IL-water mixture can be calculated as

$$\text{Weight loss}\ (\%) = \frac{m_o - m_r}{m_o} \times 100 \tag{2}$$

where m_o is the weight of the water hyacinth sample used and m_r is the weight of the residue obtained. This loss in weight (%) refers to the biomass dissolved (%) during the dissolution process.

3. Recovery of Lignin

To the filtrate obtained after treatment with IL-water mixture, deionized water was added slowly as a coagulating solvent. A brown precipitate formed gradually which could be settled by centrifugation for 15 minutes. It was washed using deionized water under vacuum filtration and then dried and weighed. From FTIR spectroscopic analysis using PERKIN Elmer System 2000, the brown precipitate was found to be lignin, while a part of it was pseudo-lignin. Based on the Klason lignin content of the native biomass, lignin yield can be determined using following equation [15],

$$\text{Lignin yield}\ (\%) = \frac{m_{precipitate}}{m_{klason\ lignin}} \times 100 \tag{3}$$

4. Characterization

XRD analysis of untreated and pretreated samples was carried out with an X-ray diffractometer [JDX-11P-3A, JEOL, Japan]. Crystallinity index (CrI) of each sample can be expressed from the following equation,

$$\text{CrI} = \frac{I_{cr} - I_{am}}{I_{cr}} \times 100 \tag{4}$$

where I_{cr} and I_{am} denote the maximum intensity of crystalline region and amorphous region, respectively.

Scanning electron microscopic analysis [FESEM, LEO 1427 VP, UK] was used to compare the surface properties of untreated biomass and regenerated biomass after treatment with IL-water mixture. To examine the presence of chemical functional groups in the recovered lignin, Fourier transform infrared (FTIR) spectroscopic analysis was carried out [PERKIN Elmer, System 2000]. Thermal stability and decomposition of recovered lignin was determined using thermogravimetric analysis (TGA) [TGA, Perkin Elmer PC Series] under nitrogen environment, which reveals the weight loss percentage of samples with respect to the temperature of thermal degradation.

Fluorescence analysis of the untreated biomass and biomass treated with the four IL-water mixtures at optimized conditions involved using a fluorescence spectrophotometer [FLUOROLOG-3, HORIBA instruments]. Fluorescence is an important and easily measurable analytical property of lignocellulosic materials because of the autofluorescence property of plant cell walls due to the presence of some endogenous fluorophores, particularly the aromatic molecules: monolignols in lignin (coniferyl alcohol, p-coumaryl alcohol, sinapyl alcohol), ferulic acid and cinnamic acid of hemicelluloses [34]. Although the three monolignols of lignin are non-conjugated moieties but exhibit high fluorescence [35]. The fluorescence property of plant cell wall depends on the composition of lignin, linkage type among monolignols and surrounding environment [36].

5. Solubility Parameters of IL-water Mixtures and Lignin

5-1. Measurements of Intrinsic Viscosity

Using an Ubbelohde viscometer, the intrinsic viscosities of IL-water mixtures were measured at different dissolution temperatures ranging from 298 K to 363 K [30,33]. The solutions of IL-water mixture in different solvents were prepared for five concentrations (0.5-5 vol%) for which efflux times were measured at least five times. Then using efflux times, the specific viscosity $\left(\eta_{sp} = \frac{t_{solution} - t_{solvent}}{t_{solvent}}\right)$ and the relative viscosity $\left(\eta_r = \frac{t_{solution}}{t_{solvent}}\right)$ of the solutions were determined and were fitted into the Huggins and Kraemer relationships given by Eqs. (5) and (6), respectively. Then from the common intercept of both equations, the intrinsic viscosity (η, dLg^{-1}) was calculated.

$$\frac{\eta_{sp}}{C} = \eta + K_H \eta^2 C \tag{5}$$

$$\frac{\eta_r}{C} = \eta + K_K \eta^2 C \tag{6}$$

where K_H and K_K are the Huggins and Kraemer constants, respectively, and C represents the concentration of the solution (IL-water mixture).

5-2. Determination of Hildebrand Solubility Parameter

The Hildebrand solubility parameters of IL-water mixtures were determined by plotting intrinsic viscosities against Hildebrand solubility parameter of different solvent and fitting by Mangaraj Equation,

$$\eta = \eta_{max} \exp[-A(\delta_{solvent} - \delta_{sample})^2] \tag{7}$$

where η_{max} denotes maximum intrinsic viscosity value, A is constant, while $\delta_{solvent}$ and δ_{sample} represent the Hildebrand solubility

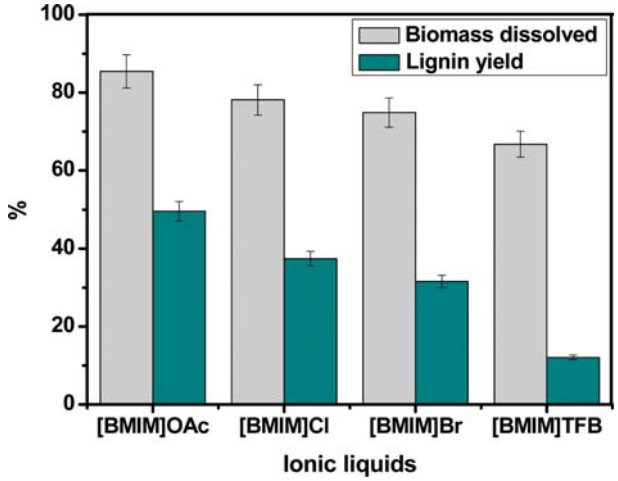

Fig. 2. Effect of ionic liquid anion on biomass dissolved (%) and lignin yield (%) during biomass dissolution in IL-water mixture.

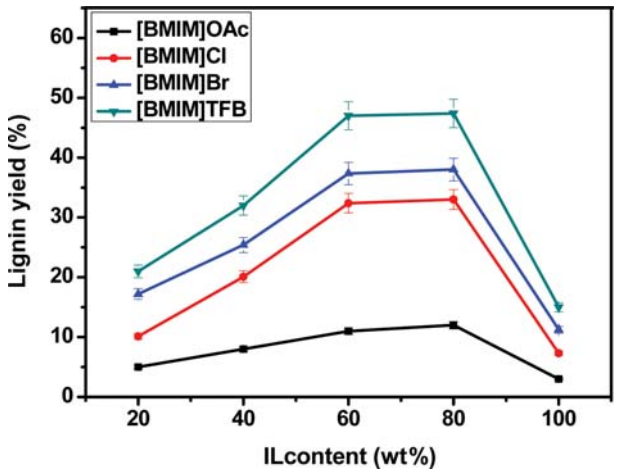

Fig. 3. Effect of ionic liquid content on lignin yield during biomass dissolution in IL-water mixture.

parameter of different solvent and IL-water mixture correspondingly. η_{max}, δ_{sample} and A can be determined from curve fitting using Origin Pro 8 Program.

RESULTS AND DISCUSSION

1. Effect of IL Anion on Biomass Dissolution

During pretreatment, interaction takes place between the ILs and lignocellulosic components, which leads to the breaking of the complex network of lignocelluloses and solubilizes the lignocellulosic components. The interactions involved are mainly ionic, π-π and hydrogen bonding, which can be attributed to the characteristics of the ILs. Fig. 2 represents the effect of different anions on percent of biomass dissolved and on yield of lignin recovered. The highest dissolution was obtained using acetate as the anion followed by chloride, bromide and TFB, respectively. The nature of the anions of IL has an intense effect on biomass dissolution and lignin recovery.

Yield of lignin recovered on pretreatment signifies the extent of lignin solubility in IL-water mixtures. Experiments were carried out at 363 K using four different ILs-water mixtures with an ionic liquid content of 60 wt%. Fig. 2 shows that biomass dissolution as well as lignin yield is found to be maximum for [BMIM]OAc-water mixture. From the figure it is observed that although the anion of ILs has not much effect on total biomass dissolved but has intense effect on lignin yield. The yield of lignin is practically found to much less using [BMIM]TFB-water mixtures, which is consistent with the results obtained later on studying the Hildebrand solubility parameters of ILs and lignin. A number of studies have reported about the considerable effect of anions of ILs on lignin solubility and thus the yield of lignin in the IL-water mixtures [21,24]. ILs such as [BMIM]OAc having moderate hydrogen bond basicity (β, 1.18) are favorable for lignin dissolution due to greater interactions among the acetate anion and lignin. While [BMIM]TFB having smaller hydrogen bond basicity (β, 0.39) results in smaller hydrogen bond interactions among BF_4^- and lignin molecule, and this explains the lignin insolubility in [BMIM]BF_4^--water mixture [37,38].

2. Influences of IL Content of IL-water Mixture in the Dissolution Process

The influence of IL content on dissolution of biomass using four different ILs-water mixtures was investigated and results are as indicated in Fig. 3. It is observed that the dissolution of biomass (%) increases on increasing the IL content from 20 wt% to 40 wt%. The dissolution of biomass (%) is found to be maximum with an IL content of 40-60 wt% for all the mixtures. However, biomass dissolved percentage decreases on using pure ionic liquid.

Thus, addition of water has a crucial role during dissolution of lignocelluloses in IL, and it is also essential to add appropriate water content to the IL during the dissolution process. The interaction among lignocellulosic components ions of ionic ILs leads to the dissolution of lignocellulosic biomass in the IL-water mixtures. Molecular dynamic simulation study on characteristics of alkyl imidazolium based IL-water mixtures proposes that with increase in water content above 70 mol% (~20 wt%) diffusion constant of the ions increases considerably while it increases more rapidly as water content reaches approximately 85% [39]. Besides this, adding water to the IL also enhances the mobility of anions and cations of the IL [40]. On adding appropriate amount of water, the water molecules fill the space above and below the imidazolium rings and reduces the strength of the cationic stacking interactions, which releases more IL ions from the stack, resulting in an increase in the interactions between the lignocellulosic components and ILs [41]. While on adding lesser water content (<50 wt%) to IL, it results in the exclusion of excess water molecules and that retards lignin dissolution. However, further investigation and analysis is required to clearly understand the interaction mechanism of IL-water mixture and lignocellulosic components.

3. Temperature Effect

Fig. 4(a) indicates the effects of temperature on treating water hyacinth using [BMIM]OAc-water (IL content of 60 wt%) for 4 h over a temperature range of 303-393 K. The biomass dissolved tends to increase rapidly from 45 wt% to 83 wt% on increasing temperature from 303 K to 363 K. While a tremendous increase in lignin yield is also observed from 17 to 44 wt% over a temperature range

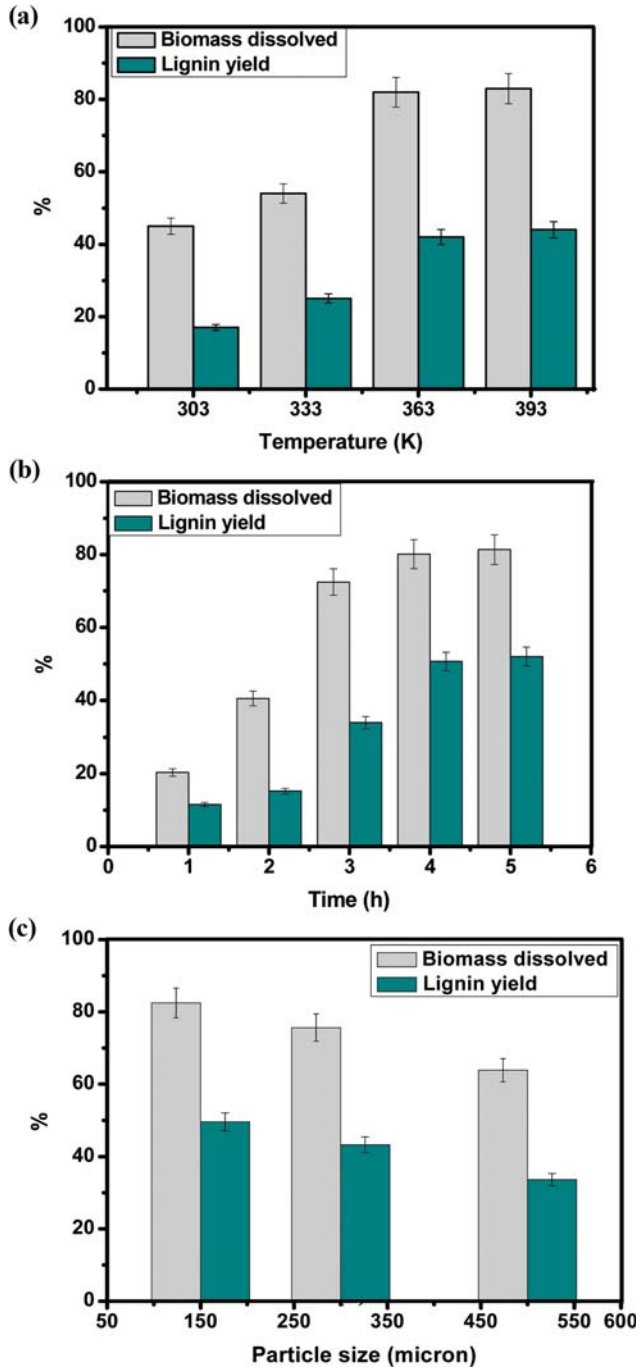

Fig. 4. Effect of (a) temperature (b) time and (c) particle size of biomass on biomass dissolved and lignin yield during dissolution in IL-water mixture.

of 303-393 K. With increasing temperature, swelling capacity and rate of dissolution of lignocelluloses in ionic liquids increases, which can be attributed to the destabilization effect of temperature on the hydrogen bonding in the lignocellulosic matrix [42,43]. A probable explanation for the higher operating temperature required for higher lignin yield is that greater amount of energy is necessary to disrupt the strong intermolecular forces and cleavage present amongst the lignin molecules [44]. Thus, a conclusion can be derived that high temperature favors higher lignin dissolution due to greater disruption of the cell structure. The optimum operation temperature for dissolution of water hyacinth using IL-water mixtures using open mode system lies below 423 K, since increasing temperature causes loss of process efficiency (biomass dissolution). This can be inferred from studies carried out by Wei et al. [22] where they concluded that vapor-liquid phase equilibrium exists at high temperature in the open mode pretreatment system of legume straw over a temperature range of 323-443 K, causing difficulty in achieving a stable operation condition above 423 K.

Table 1. Optimum conditions for the pretreatment of water hyacinth in IL-water mixtures

Parameters	Optimum conditions	Lignin yield (wt%)
Ionic liquid	[BMIM]OAc	
Ionic liquid content	60 wt%	
Temperature	363 K	50 wt%±1
Time	4 h	
Biomass particle size	150 micron	

4. Dissolution Time Effect

Fig. 4(b) illustrates the effects of time on treating water hyacinth using [BMIM]OAc-water (IL content of 60 wt%) at temperature of 363 K over a duration of 1-5 h. Biomass dissolution is found to be only 40 wt% until 2 h, which increases rapidly to about 80 wt% as duration of time increases to 4 h. From the figure it is observed that on treating biomass for 1 h minimum lignin yield of 12 wt% is obtained. Thus, it can be concluded that long pre-treatment times favor cracking the cell structure of biomass, resulting in greater dissolution of biomass and lignin yield. With increasing pretreatment time, the diffusion of IL into the biomass also increases. It can also be expected that the dissolution time can be reduced by applying higher temperature, keeping the balance with the IL-water mixtures stable.

5. Biomass Particle Size Effect

Particle size of biomass has a crucial role in the dissolution process because it has direct impact on the contact and diffusion of IL into the lignocellulosic components, which results in the solubilization of biomass [45]. Fig. 4(c) illustrates the effects of biomass particle size (150-500 micron) on treating water hyacinth using [BMIM]OAc-water mixture (IL content of 60 wt%) at 363 K over 4 h. From Fig. 4(c) it is observed that it is easy to dissolve biomass having small particle sizes in IL-water mixtures, which results in a higher amount of lignin yield. This is because of combined factors including the increased surface area of the smaller biomass particles and also due to the disruption of the complex structure of the biomass during the increase in mechanical pulping necessary to obtain smaller particles [46]. The optimum conditions of various process parameters obtained from this study during the dissolution of water hyacinth in IL-water mixtures are given in Table 1.

6. Characterizations

6-1. X-ray Diffraction

The XRD analysis of the untreated biomass and regenerated biomass after pretreatment with the four IL-water mixtures was carried out to examine and compare the crystallinity of the samples. As shown in Fig. 5, two characteristic diffraction peaks of cellulose

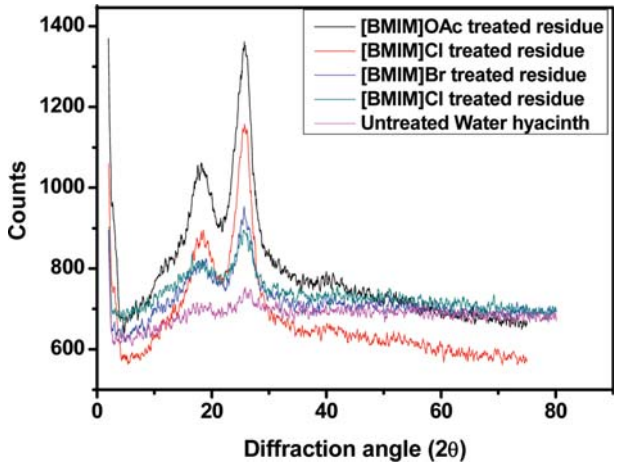

Fig. 5. XRD curves of untreated water hyacinth and residues of water hyacinth after treatment with the IL-water mixtures.

Table 2. Crystallinity indices of untreated water hyacinth and residues of water hyacinth after treatment with IL-water mixtures

Sample	Crystallinity index (%)
Untreated water hyacinth	17
Water hyacinth treated with [BMIM]OAc-water mixture	34
Water hyacinth treated with [BMIM]Cl-water mixture	31
Water hyacinth treated with [BMIM]Br-water mixture	29
Water hyacinth treated with [BMIM]TFB-water mixture	23

are observed for the untreated water hyacinth, and the IL-water treated water hyacinth at around 2θ=16.5° and 24° corresponds to (101) and (002) lattice planes of crystalline cellulose. From this study it is observed that IL-water pretreatment induced some changes in the peak which is depicted in the XRD patterns at the value of 2θ angle. Table 2 lists the crystallinity indices of the untreated biomass and the regenerated biomass after pretreatment. From Table 2, the untreated water hyacinth exhibits a lower crystallinity index value (CrI=17%) in comparison to the ILs treated water hyacinth. Crystallinity index of the biomass regenerated after treatment with [BMIM]OAc-water mixture was found to be the highest (CrI=34%) followed by [BMIMI]Cl-water (CrI=31%), [BMIMI]Cl-water

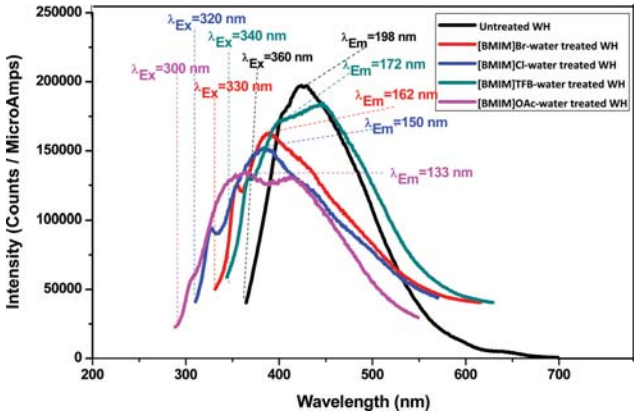

Fig. 6. X-ray fluorescence spectra of untreated water hyacinth and water hyacinth pretreated with different ILs.

(CrI=29%) and [BMIMI]Cl-water (CrI=23%). The main reason behind the increase in crystallinity of the biomass regenerated after pretreatment with IL-water mixture is due to the removal of lignin and hemicelluloses fraction (amorphous constituents) during the pretreatment process [47,48]. While a notable dissimilarity in the crystallinity index of the regenerated biomass after treatment with different IL-water mixtures is due to the differences in the capability of the ILs to dissolve the biomass. The pattern of the crystallinity indices value obtained from the XRD profile of the untreated and pretreated water hyacinth using various IL-water mixtures, it has been proved that IL-water mixture plays a significant role in the dissolution of lignin of water hyacinth samples. The order of decrease in crystallinity indices values is also consistent with the lignin dissolution capability of the four IL-water mixtures, which will be discussed in later section of this paper.

6-2. X-ray Fluorescence (XRF) Analysis

X-ray Fluorescence analysis explains the loss in fluorescence intensity observed after treating the biomass samples with different IL-water mixtures. It is observed from Fig. 6 that a noticeable decrease in the fluorescence intensity is observed for biomass samples treated with IL-water mixtures compared to the untreated biomass. This loss in the fluorescence intensity can be attributed to the decrease in the autofluorescence property of lignin due to the removal of lignin content during the pretreatment process. However, there is no noticeable difference in the fluorescence intensity among the biomass samples treated with different IL-water mix-

Table 3. Fluorescence intensity and respective excitation (λ_{EX}) and emission (λ_{EM}) wavelengths of untreated water hyacinth and IL treated water hyacinth; $\Delta_{IL\text{-}water\ treated/untreated}$: variation between IL-water treated biomass and untreated biomass

Samples	λ_{EX} (nm)	$\Delta\lambda_{EX,\ IL\text{-}water\ treated/untreated}$ (nm)	λ_{EM} (nm)	$\Delta\lambda_{EM,\ IL\text{-}water\ treated/untreated}$ (nm)	Maximum fluorescence intensity $\times 10^3$ (Counts/MicroAmps)	ΔMaximum fluorescence intensity$_{,\ IL\text{-}water\ treated/untreated}$ (%)
Untreated water hyacinth	360	-	425	-	198	-
[BMIM]TFB-water treated water hyacinth	340	−20	405	−20	172	−13%
[BMIM]Br-water treated water hyacinth	330	−30	390	−35	162	−18%
[BMIM]Cl-water treated water hyacinth	310	−50	380	−45	150	−24%
[BMIM]OAc-water treated water hyacinth	300	−60	360	−65	133	−33%

tures. Table 3 explains the variation in maximum excitation wavelength (λ_{EX}) and emission wavelength (λ_{EM}) of the samples depending on pretreatment severity of the different IL-water mixtures and depicts important decrease of both parameters ($\Delta_{IL\text{-}water}$ treated/untreated), i.e., λ_{EX} is shifted from −20 to −60 nm, while λ_{EM} undergoes variation from −20 to −65 nm indicating a blue shift. Thus, biomass samples have a different fluorescence profile depending on the pretreatment efficiency of different ILs. Thus, XRF analysis proves that pretreatment of biomass with IL-water mixture leads to the decrease in fluorescence intensity (hypochromic effect) and to a blue shift of both λ_{EX} and λ_{EM} (hypsochromic shift).

The fluorescence loss appearing in the IL treated biomass samples can be ascribed to the degradation of lignin inter-unit linkage (β-aryl-ether linkages) during the pretreatment with IL-water mixtures, which results in higher dissolution of lignin in the pretreatment process [36].

6-3. SEM Analysis

Surface morphology of the untreated water hyacinth and the sam-

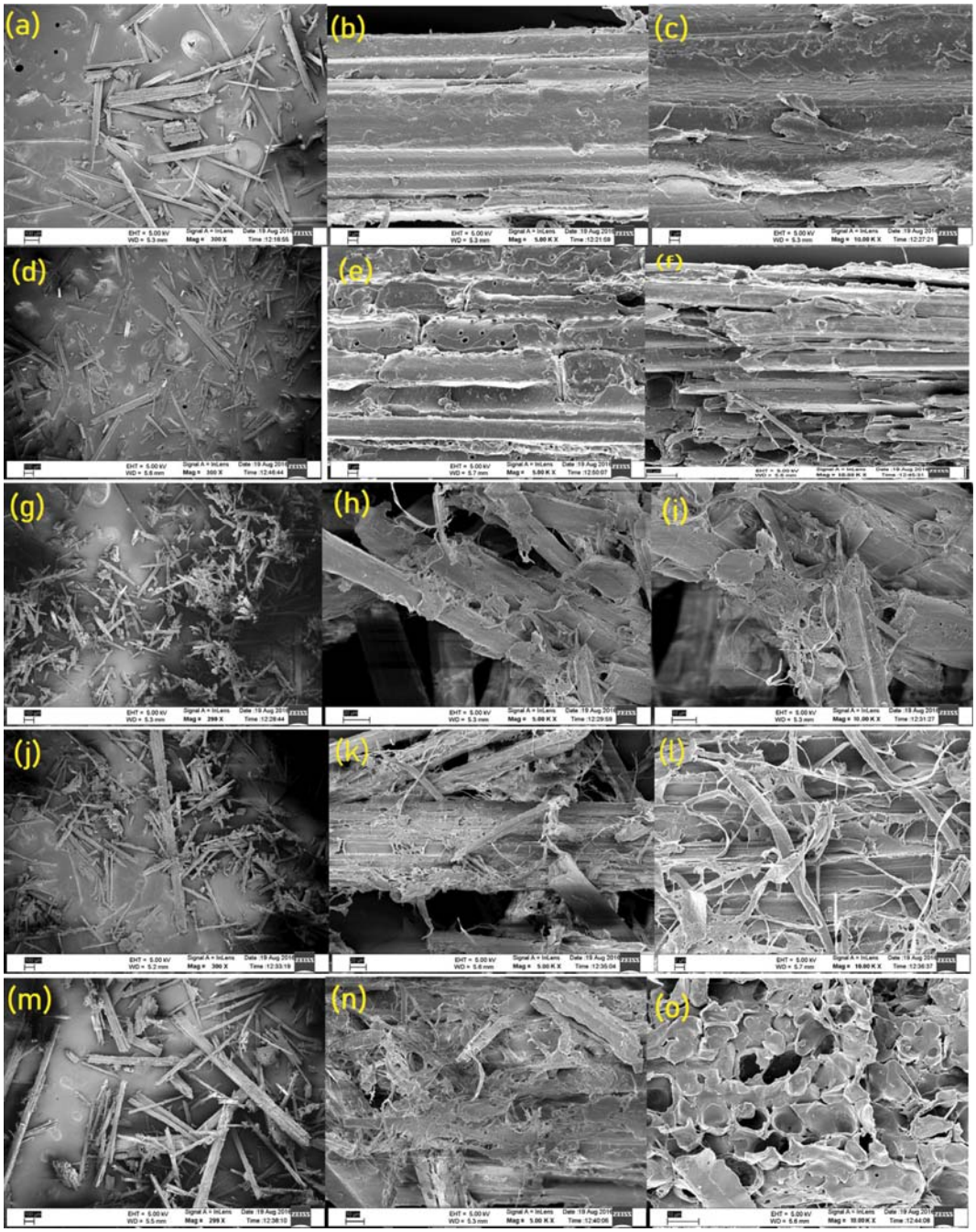

Fig. 7. SEM images of water hyacinth at magnification (300×, 5000×, 10000×); (a)-(c) untreated water hyacinth; (d)-(f) [BMIM]TFB-water treated water hyacinth; (g)-(i) [BMIM]Br-water treated water hyacinth; (j)-(l) [BMIM]Cl-water treated water hyacinth; (m)-(o) [BMIM]OAc-water treated water hyacinth.

ple regenerated after treating water hyacinth with the different IL-water mixture was studied by SEM analysis as shown in Fig. 7(a)-(o) with different levels of magnification (300×, 5000× and 10000×). SEM observations of untreated water hyacinth [Fig. 7(a)-(c)] and ionic liquid-water treated water hyacinth [Fig. 7(d)-(o)] samples show that pretreatment induces physical changes in morphology of biomass. SEM image analysis revealed smooth, tightly random surface and intact morphology [Fig. 7(a)-(c)] of the untreated biomass while pretreated samples showed a disordered and loose surface [Fig. 7(d)-(o)] caused by the IL-water mixture. Among all the pretreatments, the [BMIM]OAc-water mixture was found to be highly effective for pretreatment of water hyacinth which had altered the structure of biomass to swollen and loose and fibrous structure was transformed into porous form and been disrupted significantly [Fig. 7(m)-(o)]. Pretreatment using [BMIM]Cl-water [Fig. 7(j)-(l)] seems to have similar effects on water hyacinth, leading to the disruption of the water hyacinth after [BMIM]OAc-water. SEM analysis showed pretreatment with [BMIM]Br-water to have lesser effect on surface morphology of water hyacinth [Fig. 7(g)-(i)], while [BMIM]TFB-water was found to be incapable of making any significant alterations on biomass physical structure [Fig. 7(d)-(f)]. Results obtained from the SEM analysis clearly agree with the findings observed in case of XRD and XRF analysis. This finding indicates that on treating the biomass with IL-water mixture the intact structure of the biomass is dramatically disrupted, leading to the release of lignocellulosic components. Due to the solvating action of IL-water mixture swelling of the lignocellulosic components occurs after pretreatment, which leads to the disruption of the pretreated biomass [39].

6-4. FTIR Analysis

On comparing the FTIR spectrum of lignin recovered from water hyacinth with that of the standard lignin (alkaline), a close similarity of the two spectra is obtained as shown in Fig. 8: the relatively large and broad absorption peak (2,995-4,000 cm^{-1}) represents the hydroxyl groups in the alcohol and phenol moieties existing in the lignin. The small peaks appearing at ~2,936 and

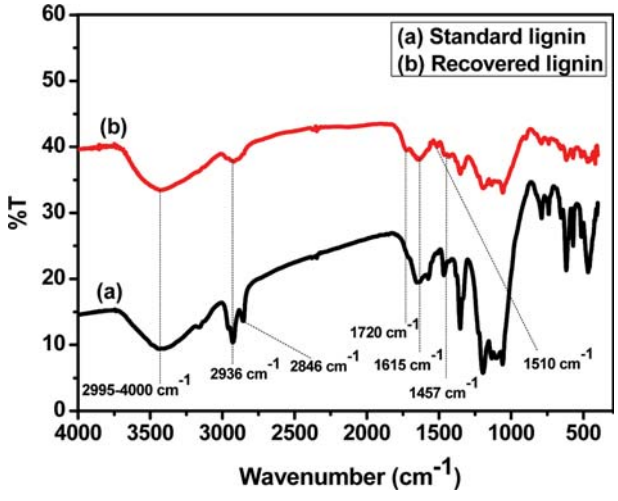

Fig. 8. FTIR spectra for (a) Standard lignin (alkaline) and (b) lignin recovered from dissolved water hyacinth in [BMIM]OAc-water mixture.

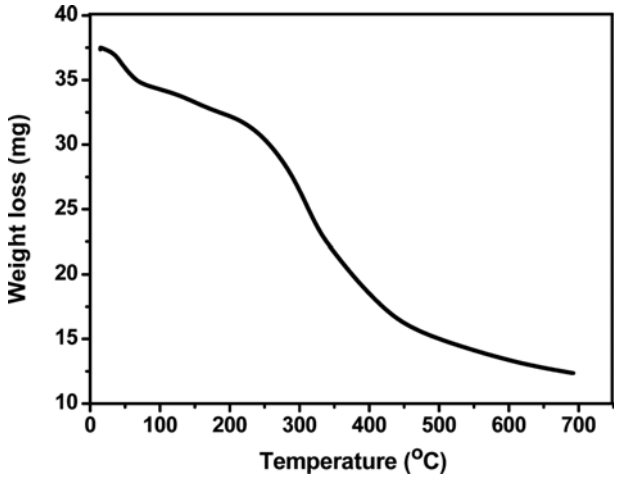

Fig. 9. TGA plot of lignin recovered from dissolved water hyacinth in [Bmim]OAc-water mixture.

2,846 cm^{-1} correspond to sp^3 -CH_3 stretching. The small absorption band appearing at ~1,720 and 1,615 cm^{-1} corresponds to the carbonyl peaks existing in the β position and in the α and γ positions of phenylpropane unit of lignin [49]. The absorption band at 1,510 cm^{-1} indicates the presence of C=C vibration in aromatic ring of lignin, while the peak at ~1,457 cm^{-1} indicates C-H asymmetric bending of CH_3 and methoxy (-OCH_3) group present in lignin.

6-5. TGA Analysis

Fig. 9 represents the TGA curve of recovered lignin as a function of temperature from which thermal properties of the extracted lignin can be evaluated. The molecular structure of lignin primarily consists of aromatic rings having several branchings, which leads to a broad range of degradation temperature from 100 to 800 °C [50]. Degradation of lignin sample can be categorized into three phases with an initial weight loss of about 2-3% occurring at 30-120 °C owing to the removal of moisture [51]. The second phase involves primary weight loss beyond 200 °C because of the removal of carbohydrate components of the lignin sample. Then, the third phase of lignin degradation occurred above 350 °C, which is the consequence of degradation of volatile products of lignin such as phenolics, alcohols, aldehydes and other gaseous products formed [52]. From the TGA curve, it is observed that thermal degradation did not commence until the sample absorbed a certain amount of heat energy. Thus on initiating heat, breaking down of lignin structure occurs causing molecular chains to be broken and degradation of lignin occurs. However, it can be suggested that lignins' thermal properties are dependent on their source.

7. Hildebrand Solubility Parameter of IL-water Mixtures and Biomass Components

Determination of the solubility parameters allows better interpretation and understanding of the intermolecular interactions among solvent and solute molecules which is responsible for the solvation process. Hildebrand solubility parameter determined by intrinsic viscosity measurement method contributes to the interpretation of the solubility properties of solvents for biomass dissolution process. Thus, Hildebrand solubility parameters offer the primary information for choosing the appropriate solvent for the

biomass dissolution process.

Taking into account the influences of the anion of ILs on the Hildebrand solubility parameters, the four different IL-water mixtures at a dissolution temperature of 298 K follow the order as, δ_H [BMIM]Cl-water, (60-40 wt%)]=25.12 $MPa^{1/2}$<δ_H [BMIM]Br-water, (60-40 wt%)]=25.68 $MPa^{1/2}$<δ_H [BMIM]OAc-water, (60-40 wt%)]= 26.97 $MPa^{1/2}$<δ_H [BMIM]TFB-water, (60-40 wt%)]=29.79 $MPa^{1/2}$ while the Hildebrand solubility parameter of lignin is found to be δ_H (lignin)=26.3 $MPa^{1/2}$. According to Hildebrand's theory of solubility parameter, the solubility of a solute in a solvent mainly depends on the criterion that they should possess significantly similar solubility parameters, i.e., the solvent having similar range of Hildebrand solubility parameters with that of the biomass component lignin, can be a suitable solvent for lignin dissolution [28]. The Hildebrand solubility parameters of IL-water mixtures were determined by plotting intrinsic viscosities against the Hildebrand solubility parameter of the different solvent and curve fitting by Mangaraj Equation (Eq. (7)). Graphs are provided in the supporting information (Fig. S1-Fig. S12).

The finding from this study indicates that compared with the δ_H of lignin (26.3 $MPa^{1/2}$), the δ_H of IL-water mixture of [BMIM]OAc-water, (60-40 wt%)] is similar, which designates [BMIM]OAc-water mixture as an outstanding solvent for dissolution and extraction of lignin. This result is in accordance with the maximum yield of lignin achieved during the dissolution of water hyacinth in IL-water mixtures, indicating the maximum solubility of lignin in this mixture of solvent. From this study, it may be concluded that determination of the Hildebrand solubility parameter offers a suitable platform to pick the appropriate solvent and gives an explanation for the dissolution behavior of biomass components.

Table 4 lists the physicochemical properties of all four IL-water mixtures as well as lignin: density, molar volume, Hildebrand solubility parameter, cohesive energy density, molar internal energy, and enthalpy of dissolution. The cohesive energy density, molar internal energy, and enthalpy of dissolution of the mixtures were calculated from Eq. (1) using Hildebrand solubility parameters, molecular weights and density mentioned in Table 4. The molar internal energy and enthalpy of dissolution of imidazolium based ILs differ in the ranges of 65.00-127.00 KJ/mol and 68.00-129.00 KJ/mol, respectively. The IL containing tetrafluoroborate as anion has greater molar internal energy and dissolution enthalpy than the other ILs, which corresponds to the observation that Hildebrand solubility parameter of IL having tetrafluoroborate is higher than the others. However, molar internal energy depends on both Hildebrand solubility parameter and molar volume.

Investigations were also carried out to study the influence of dissolution temperature on solubility parameters of IL-water mixtures. It is observed from Table 4 that on raising temperature from 298-363 K, the Hildebrand solubility parameters of different IL-water mixtures decreases in the range of 29.8-24.14 $MPa^{1/2}$. The total Hildebrand solubility parameter can be defined in terms of partial solubility parameter consisting of dispersion, polar and hydrogen bonding contributions [53]. Among these parameters, hydrogen bonding interactions are responsive to temperature, which causes weakening of hydrogen bonding on raising temperature. As a result, the hydrogen bonding solubility parameter decreases more quickly contributing to a decrease in the total solubility parameters of IL-water mixtures [54].

CONCLUSION

Water hyacinth (*Eichornia crassipes*) was pretreated with ionic-liquid (IL)-water mixture using ILs, 1-butyl-3-methylimidazolium acetate ([BMIM]OAc), 1-butyl-3-methylimidazolium chloride ([BMIM]Cl), 1-butyl-3-methylimidazolium bromide ([BMIM]Br) and 1-butyl-3-methylimidazolium tetrafluoroborate ([BMIM]TFB). Utilization of IL-water mixture as a pretreatment solvent for the LCB can be considered as an advanced step towards improved process of dissolving LCB since addition of water to the IL decreases the viscosity and process cost and enhances the ease of recyclability of the IL. Dissolution parameters such as IL content, dissolution time, temperature and biomass particle size were found to have

Table 4. Solubility properties of different IL-water mixtures and solute (lignin)

Chemical	Dissolution temperature (K)	Density (gcm^{-3})	Molecular weight ($gmol^{-1}$)	Molar volume (cm^3mol^{-1})	δ_H ($MPa^{1/2}$)	CED (Jcm^{-3})	ΔU ($kJmol^{-1}$)	ΔH ($kJmol^{-1}$)
[BMIM]OAc-water (60-40 wt%)	298	1.011	126.156	124.783	26.97	727.38	90.76	93.24
[BMIM]OAc-water (60-40 wt%)	313	0.998	126.156	126.408	26.65	710.22	89.78	92.38
[BMIM]OAc-water (60-40 wt%)	363	0.991	126.156	127.301	26.21	686.96	87.45	90.47
[BMIM]Cl-water (60-40 wt%)	298	1.05	112.002	106.668	25.12	631.01	67.31	69.78
[BMIM]Cl-water (60-40 wt%)	313	1.024	112.002	109.376	24.51	600.74	65.71	68.31
[BMIM]Cl-water (60-40 wt%)	363	1.001	112.002	111.890	24.14	582.74	65.20	68.15
[BMIM]Br-water (60-40 wt%)	298	1.279	138.672	108.422	25.68	659.46	71.50	73.98
[BMIM]Br-water (60-40 wt%)	313	1.239	138.672	111.922	25.21	635.54	71.13	73.73
[BMIM]Br-water (60-40 wt%)	363	1.208	138.672	114.794	24.89	619.51	71.12	74.14
[BMIM]TFB-water (60-40 wt%)	298	1.004	142.812	142.243	29.79	887.44	126.23	128.71
[BMIM]TFB-water (60-40 wt%)	313	0.997	142.812	143.241	29.34	860.84	123.31	125.91
[BMIM]TFB-water (60-40 wt%)	363	0.985	142.812	144.986	28.98	839.84	121.77	124.79
Alkali lignin	298	-	-	-	26.3	-	-	-

significant effects on biomass dissolution and lignin recovery. Results showed that both biomass dissolution and yield of lignin recovered were maximum for [BMIM]OAc-water mixture with an IL content of 60 wt%. Optimum lignin yield of 50 wt% was observed on dissolution of water hyacinth sample (particle size of 150 micron) with [BMIM]OAc-water mixture for 4 h at 90 °C. A theoretical interpretation using Hildebrand solubility parameter concept for selecting solvent for dissolution of lignin provided consistency in the results obtained with that of the experimental results. Thus this concept was found to be a novel theoretical interpretation to predict the appropriate IL for the dissolution of biomass so as to obtain the maximum lignin yield.

ACKNOWLEDGEMENT

Authors acknowledge CSIR New Delhi for financial support under CSC-104 and Director, CSIR-NEIST for his keen interest on this work.

SUPPORTING INFORMATION

Additional information as noted in the text. This information is available via the Internet at http://www.springer.com/chemistry/journal/11814.

REFERENCES

1. Y. S. Cheng, K. Y. Chen and T. H. Chou, *Bioresour. Technol.*, **176**, 267 (2015).
2. R. Lin, J. Cheng, W. Song, L. Ding, B. Xie and J. Zhou, *Bioresour. Technol.*, **182**, 1 (2015).
3. I. Bergier, S. M. Salis, C. H. B. Miranda, E. Ortega and C. A. Luengo, *Ecohydrol. Hydrobiol.*, **12**, 77 (2012).
4. R. Sindhu, P. Binod, A. Pandey, A. Madhavan, J. A. Alphonsa, N. Vivek, E. Gnansounou, E. Castro and V. Faraco, *Bioresour. Technol.*, **230**, 152 (2017).
5. X. Liu, X. Zu, Y. Liu, L. Sun, G. Yi, W. Lin and J. Wu, *BioRes.*, **13**, 2293 (2018).
6. B. Girisuta, B. Danon, R. Manurung, L. P. B. M. Janssen and H. J. Heeres, *Bioresour. Technol.*, **99**, 8367 (2008).
7. H. Im, B. Kim and J. W. Lee, *Bioresour. Technol.*, **193**, 386 (2015).
8. B. Kim, J. Park, J. Son and J. W. Lee, *Bioresour. Technol.*, **244**, 423 (2017).
9. T. H. Kim, Y. K. Oh, J. W. Lee and Y. K. Chang, *Algal. Res.*, **26**, 431 (2017).
10. L. Jouanin and C. Lapierre, *Lignins: biosynthesis, biodegradation and bioengineering*, Academic press, Netherlands (2012).
11. P. Maki-Arvela, I. Anugwom, P. Virtanen, R. Sjoholma and J. P. Mikkolaa, *Ind. Crops Prod.*, **32**, 175 (2010).
12. J. Rahikainen, S. Mikander, K. Marjamaa, T. Tamminen, A. Lappas, L. Viikari and K. Kruus, *Biotechnol. Bioeng.*, **108**, 2823 (2011).
13. A. Pinkert, D. F. Goeke, K. N. Marsh and S. Pang, *Green Chem.*, **13**, 3124 (2011).
14. R. Beauchet, F. Monteil-Rivera and J. M. Lavoie, *Bioresour. Technol.*, **121**, 328 (2012).
15. X. Han and D. W. Armstrong, *Acc. Chem. Res.*, **40**, 1079 (2007).
16. S. H. Lee, T. V. Doherty, R. J. Linhardt and J. S. Dordick, *Biotechnol. Bioeng.*, **102**, 1368 (2009).
17. K. N. Marsh, A. Deev, A. C. T. Wu, E. Tran and A. Klamt, *Korean J. Chem. Eng.*, **19**, 357 (2002).
18. D. A. Fort, R. C. Remsing, R. P. Swatloski, P. Moyna, G. Moyna and R. D. Rogers, *Green Chem.*, **9**, 63 (2007).
19. S. Xu, C. Huang, J. Zhang, J. Liu and B. Chen, *Korean J. Chem. Eng.*, **26**, 985 (2009).
20. D. B. Fu and G. Mazza, *Bioresour. Technol.*, **102**, 7008 (2011).
21. A. Brandt, M. J. Ray, T. Q. To, D. J. Leak, R. J. Murphy and T. W. Welton, *Green Chem.*, **13**, 2489 (2011).
22. L. G. Wei, K. L. Li, Y. C. Ma and X. Hou, *Ind. Crops Prod.*, **37**, 227 (2012).
23. Z. Y. Zhang, I. M. O'Hara and W. O. S. Doherty, *Bioresour. Technol.*, **120**, 149 (2012).
24. Y. Wang, L. Wei, K. Li, Y. Ma, N. Ma, S. Ding, L. Wang, D. Zhao, B. Yan, W. Wan, Q. Zhang, X. Wang, J. Wang and H. Li, *Bioresour. Technol.*, **170**, 499 (2014).
25. R. P. Swatloski, S. K. Spear, J. D. Holbrey and R. D. Rogers, *J. Am. Chem. Soc.*, **124**, 4974 (2002).
26. M. Mazza, D. A. Catana, C. Vaca-Garcia and C. Cecutci, *Cellulose,* **16**, 207 (2009).
27. Y. C. Ma, L. G. Wei, K. L. Li, S. J. Wang, J. Y. Yu and Y. L. Li, Chinese Patent, CN101580522B (2012).
28. P. Weerachanchai, K. K. Sang and J. M. Lee, *Bioresour. Technol.*, **170**, 160 (2014).
29. P. Weerachanchai, Y. Wong, K. H. Lim, T. T. Y. Tan and J. M. Lee, *Chem. Phys. Chem.*, **15**, 3580 (2014).
30. S. H. Lee and S. B. Lee, *Chem. Commun.*, **27**, 3469 (2005).
31. A. F. M. Barton, *Chem. Rev.*, **75**, 731 (1975).
32. P. Bustamante, J. Navarro-Lupion and B. Escalera, *Eur. J. Pharm. Sci.*, **24**, 229 (2005).
33. P. Weerachanchai, Z. Chen, S. S. J. Leong, M. W. Chang and J. M. Lee, *Chem. Eng. J.*, **213**, 356 (2012).
34. H. K. Lichtenthaler and J. Schweiger, *J. Plant Physiol.*, **152**, 272 (1998).
35. J. C. Dean, P. S. Walsh, B. Biswas, P. V. Ramachandran and T. S. Zwier, *Chem. Sci.*, **5**, 1940 (2014).
36. T. Auxenfans, C. Terryn and G. Paes, *Sci. Rep.*, **7**, 8838 (2017).
37. R. Lungwitz and S. Spange, *New J. Chem.*, **32**, 392 (2008).
38. T. V. Doherty, M. Mora-Pale, S. E. Foley, R. J. Linhardt and J. S. Dordick, *Green Chem.*, **12**, 1967 (2010).
39. A. A. Niazi, D. Rabideau Brooks and A. E. Ismail, *J. Phys. Chem. B*, **117**, 1378 (2013).
40. S. Stevanovik, A. Podgorsek and A. A. H. Padua and M. F. Costa Gomes, *J. Phys. Chem. B*, **116**, 14416 (2012).
41. T. Mendez-Morales, J. Carrete, O. Cabeza, L. J. Gallego and L. M. Varela, *J. Phys. Chem. B*, **115**, 6995 (2011).
42. M. Zavrel, D. Bross, M. Funke, J. Buchs and A. C. Spiess, *Bioresour. Technol.*, **100**, 2580 (2009).
43. A. Brandt, J. P. Hallett, D. J. Leak, R. J. Murphy and T. Welton, *Green Chem.*, **12**, 672 (2010).
44. T. Rashid, N. Gnanasundaram, A. Appusamy and C. F. Kait, *Ind. Crops Prod.*, **116**, 122 (2018).
45. G. Gogoi and S. Hazarika, *Sep. Purif. Technol.*, **173**, 113 (2017).

46. N. Sun, M. Rahman, Y. Qin, M. L. Maxim, H. Rodriguez and R. D. Rogers, *Green Chem.*, **11**, 646 (2009).
47. X. D. Hou, T. J. Smith, N. Li and M. H. Zong, *Biotechnol. Bioeng.*, **109**, 2484 (2012).
48. H. A. Silverio, W. P. F. Neto, N. O. Dantas and D. Pasquini, *Ind. Crops Prod.*, **44**, 427 (2013).
49. R. S. Rohella, N. Sahoo, S. C. Paul, S. Choudhury and V. Chakravortty *Thermochim. Acta*, **287**, 131 (1996).
50. H. Yang, R. Yan, H. Chen, D. H. Lee and C. Zheg, *Fuel*, **86**, 1781 (2007).
51. A. Tejado, C. Pena, J. Labidi, J. M. Echeverria and I. Mondragon, *Bioresour. Technol.*, **98**, 1655 (2007).
52. D. Watkins, Md. Nuruddin, M. Hosur, A. T. Nareth and S. Jeelani, *J. Mater. Res. Technol.*, **4**, 26 (2015).
53. M. Mora-Pale, L. Meli, T. V. Doherty, R. J. Linhardt and J. S. Dordick, *Biotechnol. Bioeng.*, **108**, 1229 (2011).
54. Y. Wong, Z. J. Chen, T. T. Y. Tan and J. M. Lee, *Ind. Eng. Chem. Res.*, **54**, 12150 (2015).

Supporting Information

Dissolution of lignocellulosic biomass in ionic liquid-water media: Interpretation from solubility parameter concept

Gayatri Gogoi*, and Swapnali Hazarika*,**,†**

*Chemical Engineering Group, Engineering Science and Technology Division (ESTD),
CSIR North East Institute of Science & Technology, Jorhat-785006, Assam, India
**Academy of Scientific and Industrial Research, CSIR NEIST Campus
(*Received 3 May 2019 • accepted 15 August 2019*)

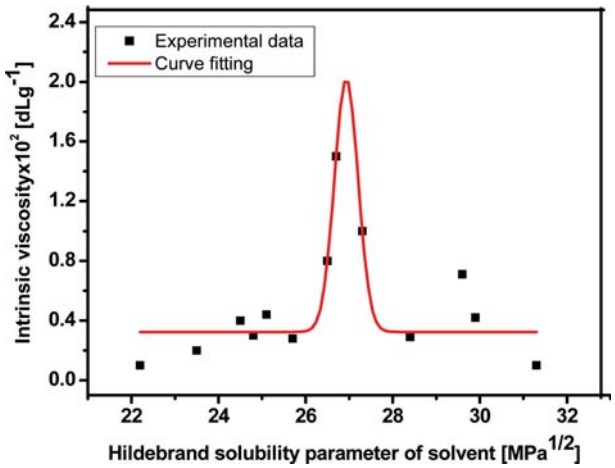

Fig. S1. Intrinsic viscosity as a function of solvent Hildebrand solubility parameter for [BMIM]OAc-water (60-40 wt%) at 298 K.

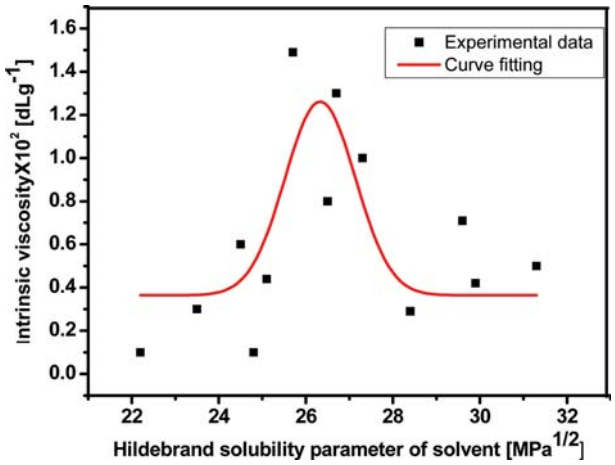

Fig. S2. Intrinsic viscosity as a function of solvent Hildebrand solubility parameter for [BMIM]OAc-water (60-40 wt%) at 313 K.

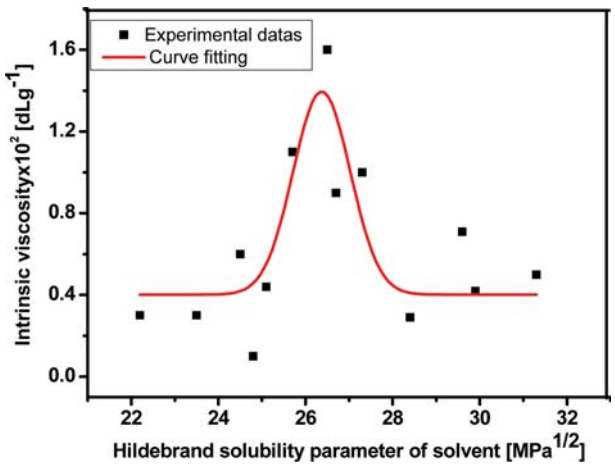

Fig. S3. Intrinsic viscosity as a function of solvent Hildebrand solubility parameter for [BMIM]OAc-water (60-40 wt%) at 363 K.

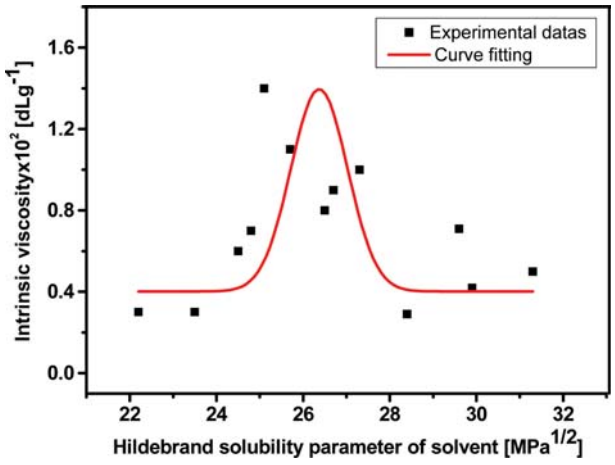

Fig. S4. Intrinsic viscosity as a function of solvent Hildebrand solubility parameter for [BMIM]Cl-water (60-40 wt%) at 298 K.

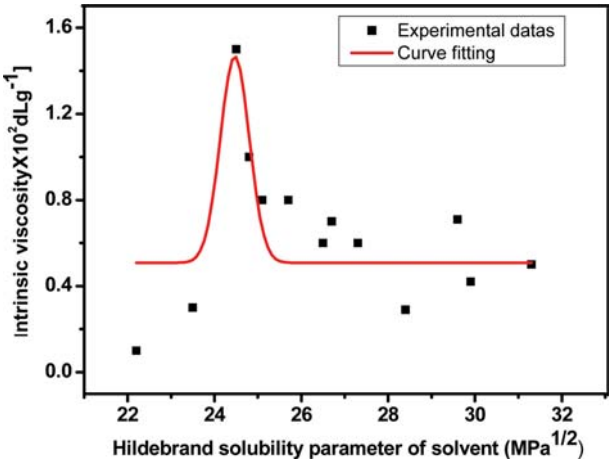

Fig. S5. Intrinsic viscosity as a function of solvent Hildebrand solubility parameter for [BMIM]Cl-water (60-40 wt%) at 313 K.

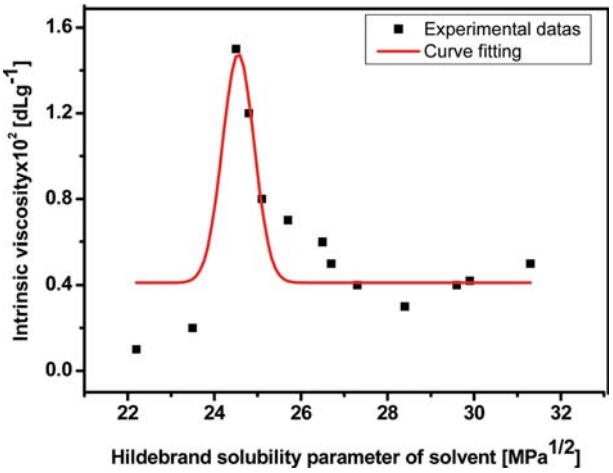

Fig. S6. Intrinsic viscosity as a function of solvent Hildebrand solubility parameter for [BMIM]Cl-water (60-40 wt%) at 363 K.

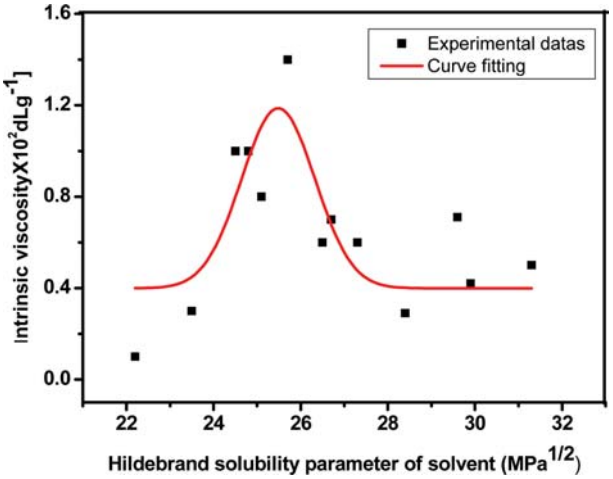

Fig. S7. Intrinsic viscosity as a function of solvent Hildebrand solubility parameter for [BMIM]Br-water (60-40 wt%) at 298 K.

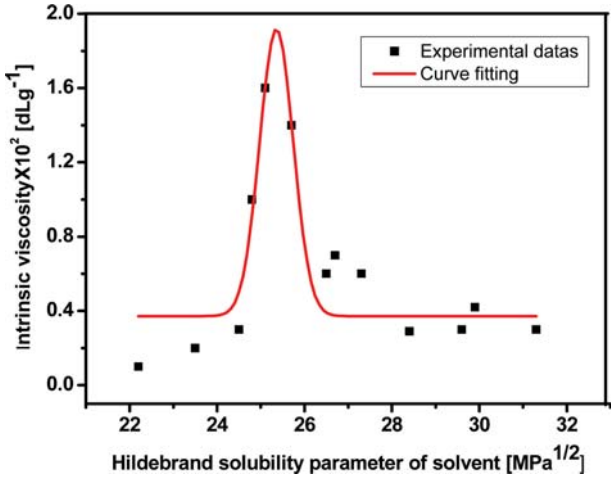

Fig. S8. Intrinsic viscosity as a function of solvent Hildebrand solubility parameter for [BMIM]Br-water (60-40 wt%) at 313 K.

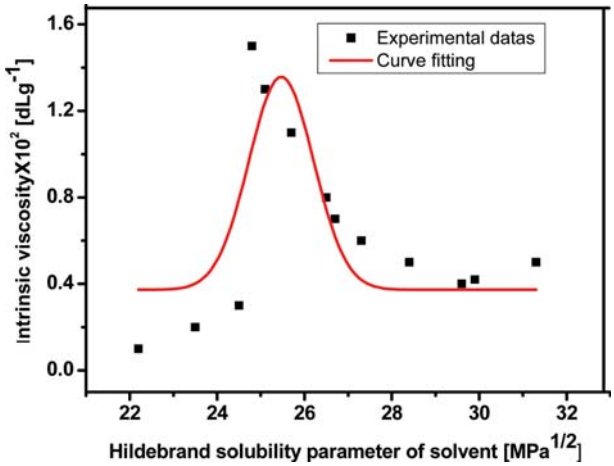

Fig. S9. Intrinsic viscosity as a function of solvent Hildebrand solubility parameter for [BMIM]Br-water (60-40 wt%) at 363 K.

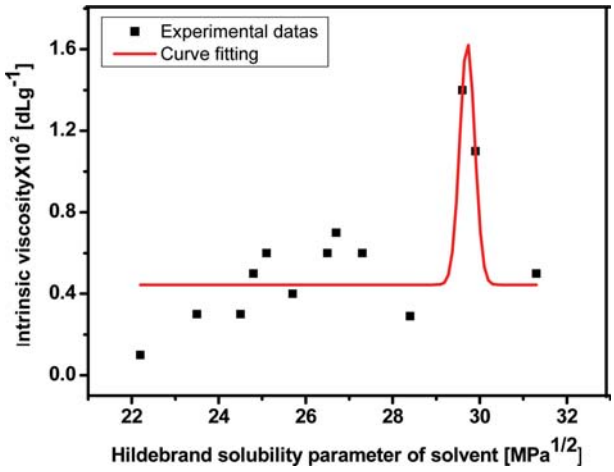

Fig. S10. Intrinsic viscosity as a function of solvent Hildebrand solubility parameter for [BMIM]TFB-water (60-40 wt%) at 298 K.

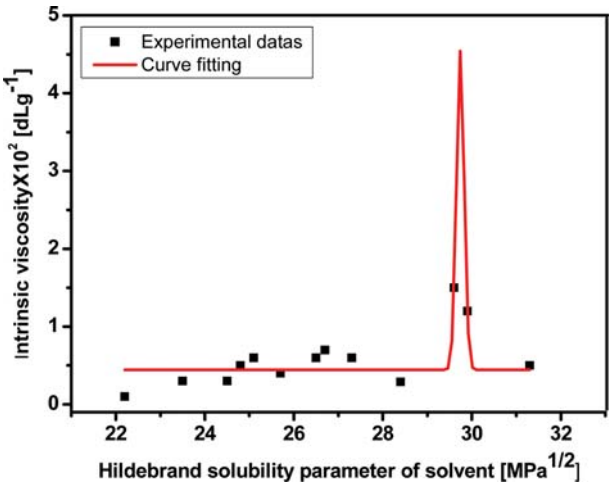

Fig. S11. Intrinsic viscosity as a function of solvent Hildebrand solubility parameter for [BMIM]TFB-water (60-40 wt%) at 313 K.

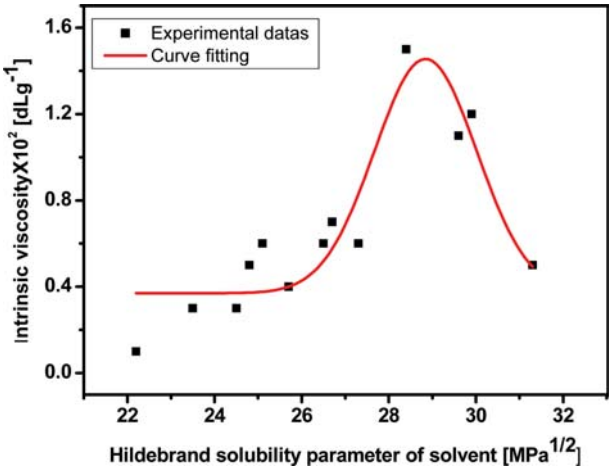

Fig. S12. Intrinsic viscosity as a function of solvent Hildebrand solubility parameter for [BMIM]TFB-water (60-40 wt%) at 363 K.

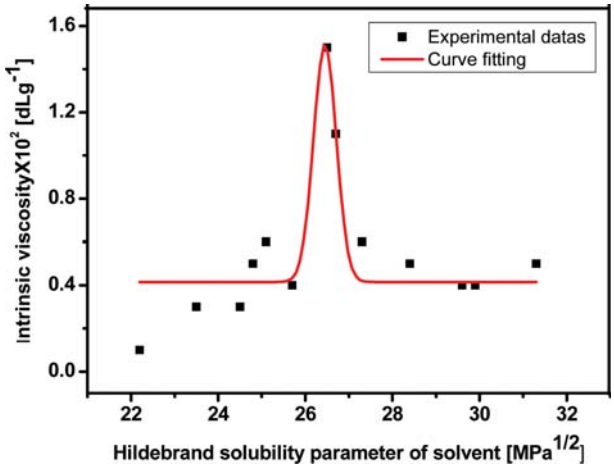

Fig. S13. Intrinsic viscosity as a function of solvent Hildebrand solubility parameter for lignin at 298 K.